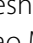


FULL PAPER

Open Access



Initial performance of the radio occultation experiment in the Venus orbiter mission Akatsuki

Takeshi Imamura^{1*} , Hiroki Ando², Silvia Tellmann³, Martin Pätzold³, Bernd Häusler⁴, Atsushi Yamazaki⁵, Takao M. Sato⁵, Katsuyuki Noguchi⁶, Yoshifumi Futaana⁷, Janusz Oschlisniok³, Sanjay Limaye⁸, R. K. Choudhary⁹, Yasuhiro Murata⁵, Hiroshi Takeuchi⁵, Chikako Hirose⁵, Tsutomu Ichikawa⁵, Tomoaki Toda⁵, Atsushi Tomiki⁵, Takumi Abe⁵, Zen-ichi Yamamoto⁵, Hiroto Noda¹⁰, Takahiro Iwata⁵, Shin-ya Murakami⁵, Takehiko Satoh⁵, Tetsuya Fukuhara¹¹, Kazunori Ogohara¹², Ko-ichiro Sugiyama¹³, Hiroki Kashimura¹⁴, Shoko Ohtsuki¹⁵, Seiko Takagi¹⁶, Yukio Yamamoto⁵, Naru Hirata¹⁷, George L. Hashimoto¹⁸, Manabu Yamada¹⁹, Makoto Suzuki⁵, Nobuaki Ishii⁵, Tomoko Hayashiyama²⁰, Yeon Joo Lee⁵ and Masato Nakamura⁵

Abstract

After the arrival of Akatsuki spacecraft of Japan Aerospace Exploration Agency at Venus in December 2015, the radio occultation experiment, termed RS (Radio Science), obtained 19 vertical profiles of the Venusian atmosphere by April 2017. An onboard ultra-stable oscillator is used to generate stable X-band downlink signals needed for the experiment. The quantities to be retrieved are the atmospheric pressure, the temperature, the sulfuric acid vapor mixing ratio, and the electron density. Temperature profiles were successfully obtained down to ~ 38 km altitude and show distinct atmospheric structures depending on the altitude. The overall structure is close to the previous observations, suggesting a remarkable stability of the thermal structure. Local time-dependent features are seen within and above the clouds, which is located around 48–70 km altitude. The H₂SO₄ vapor density roughly follows the saturation curve at cloud heights, suggesting equilibrium with cloud particles. The ionospheric electron density profiles are also successfully retrieved, showing distinct local time dependence. Akatsuki RS mainly probes the low and middle latitude regions thanks to the near-equatorial orbit in contrast to the previous radio occultation experiments using polar orbiters. Studies based on combined analyses of RS and optical imaging data are ongoing.

Keywords: Venus, Radio occultation, Akatsuki

Introduction

The main goal of the Venus orbiter mission Akatsuki is to understand the mechanisms driving the atmospheric circulation and maintaining the cloud layer (Nakamura et al. 2011). For this purpose, five cameras onboard, having bandpass filters, take images of Venus at different wavelengths to observe the horizontal distributions of clouds and minor constituents at different heights. Radio

occultation measurement in Akatsuki, termed RS (Radio Science), aims at exploration of the vertical structure of the atmosphere (Imamura et al. 2011), being complementary to the imaging observations by onboard cameras.

The orbiter was launched in May 2010 and arrived at Venus in December 2010. The first attempt on Venus orbit insertion has failed, and the second attempt conducted in December 2015, after 5-years of interplanetary cruise, was successful (Nakamura et al. 2016). Regular observations of the Venusian atmosphere with radio occultation technique have started in March 2016. In addition to the observation of Venus, radio occultation observations of the solar corona were conducted during

*Correspondence: t_imamura@edu.k.u-tokyo.ac.jp

¹ Graduate School of Frontier Sciences, The University of Tokyo, Kiban-tou 4H7, 5-1-5 Kashiwanoha, Kashiwa, Chiba 277-8561, Japan
Full list of author information is available at the end of the article

the solar conjunction periods in 2011 and 2016 using the same equipment (Imamura et al. 2014b).

Radio occultation has played a crucial role in determining the structures of the planetary atmospheres (e.g., Eshleman 1973; Tyler 1987; Pätzold et al. 2007; Imamura et al. 2012). In a radio occultation experiment conducted with a spacecraft equipped with a stable frequency source, the spacecraft transmits radio waves toward the Earth, while it goes behind the planet and reemerges as seen from the Earth. During such occultation events, the planetary atmosphere causes bending and attenuation of the radio waves. Assuming a local spherical symmetry, the analysis of the frequency and the signal intensity time series obtained at the tracking station yields vertical profiles of the refractive index and the absorption coefficient. Temperature profiles are obtained from the refractive index profiles assuming hydrostatic balance. The advantages of this technique over other remote sensing techniques are its high vertical resolution (typically < 1 km) and high temperature resolution (typically < 1 K) (Hinson and Jenkins 1995; Tellmann et al. 2009). Radio occultation can cover altitudes from the sub-cloud region (< 50 km) to the upper atmosphere (~ 90 km). The quality of the measurement declines below 40 km due to defocusing loss and absorption, and no information is obtained below ~ 32 km since the curvature of the ray path exceeds that of the planetary surface (Fjeldbo et al. 1971; Häusler et al. 2006).

The scientific background of the measurement has been described in Imamura et al. (2011); here, we briefly describe the background with recent updates. Previous radio occultation experiments of the Venusian atmosphere revealed the meridional structure of the atmospheric temperature, including the horizontally near-uniform temperature below the cloud layer, the cold collar and the mid-latitude jet at cloud heights, and the warm high latitudes above clouds (Kliore and Patel 1980; Newman et al. 1984; Piccialli et al. 2012). The dynamical stability of the atmosphere was studied using radio occultation temperatures (Piccialli et al. 2012). The static stability is near neutral in the middle and lower cloud regions (50–58 km), suggesting occurrence of vertical convection (Pollack et al. 1980; Tellmann et al. 2009). At altitudes above ~ 58 km, propagation of gravity waves is suggested from wavelike features in the temperature profiles (Hinson and Jenkins 1995; Tellmann et al. 2012; Ando et al. 2015a). In spite of these findings, the relationship among the variations of the temperature field, the wind field and the cloud distribution has not been studied. Local time dependence of the thermal structure in the cloud is also unclear, although numerical models predict significant diurnal variations (Imamura et al. 2014a).

Mixing ratios of H₂SO₄ vapor, which is concentrated in the sub-cloud region, have been retrieved from the attenuation of radio occultation signals (Jenkins et al. 1994; Kolodner and Steffes 1998; Oschlisniok et al. 2012). The observed H₂SO₄ vapor distribution suggests control of the H₂SO₄ distribution by condensation and evaporation in clouds, thermal decomposition in the lower atmosphere, and global-scale circulation (Krasnopolsky and Pollack 1994; Imamura and Hashimoto 1998, 2001). Using Venus Express radio occultation data, Oschlisniok et al. (2012) revealed complicated meridional distribution and local time dependence of the mixing ratio, which are not reproduced in numerical models. The relationship among the variations of the thermal structure, the H₂SO₄ vapor distribution, and the cloud distribution is a key to understanding the cloud system; regional cloud models predict significant variability of the clouds (McGouldrick et al. 2008a, b), and Venus Express VIRTIS showed mesoscale variability of the cloud optical thickness (McGouldrick et al. 2012).

The occurrence of small-scale atmospheric density fluctuations, having scales smaller than the Fresnel diameter given later, has been inferred from the scintillation of radio occultation signals. The scintillation, which is enhanced around 60 km altitude and at high latitudes, might be caused by turbulence (Woo et al. 1980) or gravity waves (Leroy and Ingersoll 1996). Ando et al. (2015a) argued, based on a spectral analysis of radio occultation temperatures, that saturation of gravity waves through convective instability occurs above clouds, although there is no direct evidence for wave breaking. A detailed comparison of the distribution of scintillation with wavy temperature structures might provide clues to wave breaking and resultant turbulence.

Ionospheric electron densities have primarily been measured by radio occultation technique (Kliore and Luhmann 1991). The peak electron density is an order of magnitude higher on the dayside than nightside, and multiple layers are observed on the dayside (Pätzold et al. 2007). The structure of the ionosphere is affected by the input of energy and momentum from the solar wind to the upper atmosphere, and also by the dynamical coupling with the lower neutral atmosphere. The latter is particularly unexplored and should be studied with simultaneous observations of the variability of the lower atmosphere and the upper atmosphere.

This paper presents the initial performance, the observation plan, and the expected science themes of Akatsuki RS. Scientific results will be reported elsewhere. The observation plan was largely changed from the original given in Imamura et al. (2011) because of the change of the orbit around Venus. The originally planned orbit is a 30 h-period elliptical orbit with the apoapsis altitude

of ~ 13 Venus radii, while the current orbit is a 10.5-day-period elliptical orbit with the apoapsis altitude of 59 Venus radii.

Radio occultation method

The schematic of the radio occultation measurement is shown in Fig. 1. Radio waves are transmitted from the spacecraft, refracted in the planetary atmosphere, and received at a ground station. The asymptotic bending angle α and the ray impact parameter a are calculated from the measured atmospheric Doppler shift and the reconstructed velocity and position vectors of the spacecraft and the ground station. For a radially symmetric atmosphere, the refractive index n is obtained as a function of the radius r from the relationship between α and a through Abel transformation (Fjeldbo et al. 1971):

$$\ln n(r) = -\frac{1}{\pi} \int_{a_1}^{\infty} \ln \left\{ \frac{a}{a_1} + \left[\left(\frac{a}{a_1} \right)^2 - 1 \right]^{\frac{1}{2}} \right\} \frac{d\alpha}{da} da, \tag{1}$$

where a_1 is the impact parameter for a ray whose radius of closest approach is r , and a_1 and r are related with each other through Bouguer’s rule, $n(r)r = a_1$.

The deviation of the refractive index n from unity is the sum of the contributions from the neutral atmosphere and the ionosphere:

$$n - 1 = VN \times 10^{-6} - \frac{\beta N_e}{f^2}, \tag{2}$$

where V is the refractive volume, N is the number density of the neutral atmosphere, $\beta = e^2/8\pi^2\epsilon_0 m_e \sim 40.3 \text{ m}^3 \text{ s}^{-2}$ with e , ϵ_0 , m_e being the elementary charge, the dielectric

constant in vacuum and the electron mass, respectively, N_e is the number density of electrons, and f is the frequency of the carrier signal. On the assumption that the neutral atmosphere is well mixed, we adopt a constant V of $1.811 \times 10^{-17} \text{ m}^3$ that is appropriate for the composition of 96.5% CO_2 and 3.5% N_2 based on experimental data (Essen and Froome 1951; Fjeldbo and Eshleman 1968) following Tellmann et al. (2009). The neutral and ionospheric contributions are almost separated in altitude with the boundary around 100 km altitude; this enables us to retrieve the vertical profiles of the neutral atmospheric density N and the electron density N_e separately. The vertical profile of the neutral atmospheric pressure, $p(r)$, is derived from the density profile $N(r)$ by integrating the equation of hydrostatic equilibrium:

$$p(r) = p(r_{\text{top}}) + m \int_r^{r_{\text{top}}} N(r')g(r')dr', \tag{3}$$

where m is the mean molecular mass that is taken to be 43.44 u (Seiff et al. 1985), $g(r)$ is the altitude-dependent acceleration due to gravity, and r_{top} is the upper boundary, which is taken to be around 90–100 km altitude. The product of the gravitational constant and the mass of Venus used for calculating $g(r)$ is $GM = 3.24858592 \times 10^5 \text{ km}^3 \text{ s}^{-2}$ following the value adopted in NASA’s SPICE system. The ideal gas law relates $p(r_{\text{top}})$ to the atmospheric temperature at this height, $T(r_{\text{top}})$, as $p(r_{\text{top}}) = N(r_{\text{top}})kT(r_{\text{top}})$, where k is the Boltzmann’s constant. The boundary condition $T(r_{\text{top}})$ is determined empirically. The temperature profile $T(r)$ is calculated from $N(r)$ and $p(r)$ using the ideal gas law. The influence of $T(r_{\text{top}})$ on $T(r)$ becomes negligibly small around 10 km below r_{top} (Tellmann et al. 2009). The

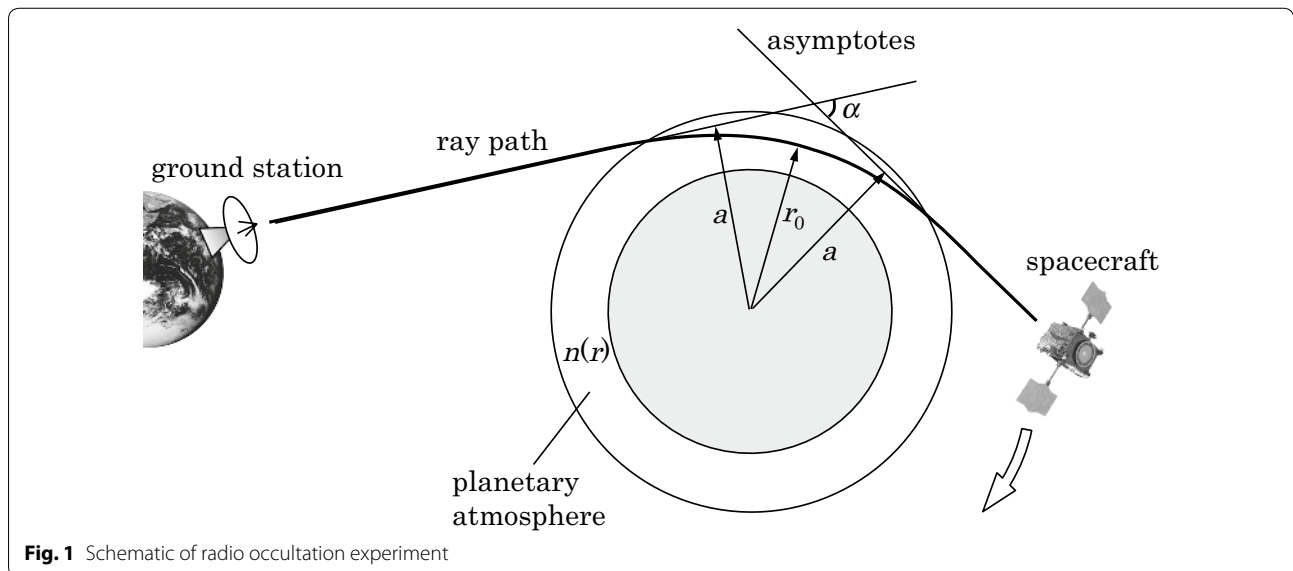


Fig. 1 Schematic of radio occultation experiment

vertical resolution is limited by the diameter of the first Fresnel zone, which is given by (Häusler et al. 2006; Imamura et al. 2011)

$$d = 2\sqrt{\lambda DL}, \quad (4)$$

where λ is the wavelength of the carrier signal, D is the distance from the spacecraft to the crossing of the ray asymptotes, and L is the defocusing loss given later. Above ~ 90 km altitude, where defocusing loss is negligible ($L = 1$), d ranges from 1.0 to 1.8 km in Akatsuki radio occultation experiments conducted by April 2017 because of the change of D in the range 7000–23,000 km. Although the distance between Akatsuki and Venus changes significantly along the orbit, radio occultation mostly occurs when the spacecraft is located near the periapsis. The d becomes smaller at lower altitudes because of the smaller L : it is 0.4–0.5 km at 75 km altitude in the same period.

When retrieving the amount of absorbing materials from the signal intensity, we first remove the contribution of atmospheric defocusing, which is caused by the radial gradient of the refractive index, from the intensity time series. The defocusing loss is estimated by (Eshleman 1973)

$$L = \left(\cos \alpha - D \frac{d\alpha}{da} \right)^{-1}. \quad (5)$$

The loss is ~ 26 dB at 40 km altitude for a typical D of 2 Venus radii (Imamura et al. 2011). The corrected intensity time series is converted to a height profile of the absorptivity with the aid of ray tracing on the assumption of a spherically symmetric atmosphere (Oschlisniok et al. 2012).

Observation system

One-way downlink at X-band (8410.932 MHz) is used in the experiment. The experiment relies on the frequency stability of both the onboard radio wave source and the recording system at the ground station. Akatsuki RS employs an ultra-stable oscillator (USO) as the onboard frequency source; the performance of the USO is given in “Performance of the ultra-stable oscillator”. The USO is almost identical to those onboard ESA’s Rosetta and Venus Express spacecraft (Häusler et al. 2007). The absence of the second frequency (such as S-band) prevents dual-frequency occultation method, which is sensitive only to plasma along the radio propagation path (e.g., Imamura et al. 2010; Pätzold et al. 2007). This might have some influence on the detection of ionospheric fine structures at low ionospheric altitudes but will not alter the coarse ionospheric electron density profiles.

The 3 dB half beam width of the high-gain antenna is $\sim 1^\circ$; since the ray bending exceeds the beam width, the spacecraft performs attitude maneuvers to compensate for the changing direction of the signal path. The direction of the antenna beam is changed along a polygonal (zigzag) curve in such a way that the difference between the controlled beam direction and the ideal beam direction based on the Venus International Reference Atmosphere (VIRA) (Seiff et al. 1985) is less than 0.05° . The difference sometimes exceeds this limit because of an inaccurate trajectory prediction at the time of command generation, leading to non-negligible decline of the signal intensity. The effect of such antenna mispointing on the measured signal intensity is corrected before analysis using the measured antenna pattern (Toda et al. 2010) and the trajectory data reconstructed after the experiment. The accuracy of this intensity correction is estimated to be better than 1 dB in most of the cases.

The accuracy of the altitudes in the derived atmospheric profiles relies on the accuracy of trajectory determination. According to the analysis of flight dynamics, the position of Akatsuki relative to Venus typically has an error of 100–500 m during radio occultation experiments. This error causes uncertainties of the altitude offset of similar magnitude in the atmospheric profiles.

The primary ground station used for the experiment is the 64-m antenna of Usuda Deep Space Center (UDSC) of JAXA, which is located at $138^\circ 21' 54''$ East longitude, $36^\circ 07' 44''$ North latitude. In addition to UDSC, for increasing the number of observation opportunities, we started to use the 32-m antenna of Indian Deep Space Network (IDSN) of Indian Space Research Organization (ISRO), which is located at $77^\circ 22' 08''$ East longitude, $12^\circ 54' 11''$ North latitude, from March 2017.

The received signals are down-converted to $< \sim 1$ MHz by an open-loop heterodyne system stabilized by a hydrogen maser (Allan deviation $< 3 \times 10^{-13}$ for 1 s, $< 3 \times 10^{-15}$ for 1000 s) and 8-bits digitized. The sampling rate is 0.5–4 MHz so that the received signal can be confined in the recording bandwidth, while the frequency changes with time due to Doppler shift. The detail of the observation system is given in Imamura et al. (2011).

Locations of observations

The orbit around Venus is a 10.5-day-period elliptical orbit near the equator (Nakamura et al. 2016). The direction of orbital motion is westward, which coincides with the direction of the atmospheric super-rotation. The apoapsis altitude is $\sim 360,000$ km, or 59 Venus radii, and the periapsis altitude is variable in the range 1000–8000 km. Figure 2 shows the latitudes and local times of the RS observation points till December 2020 plotted against the Earth days after January 1, 2016. Here, the

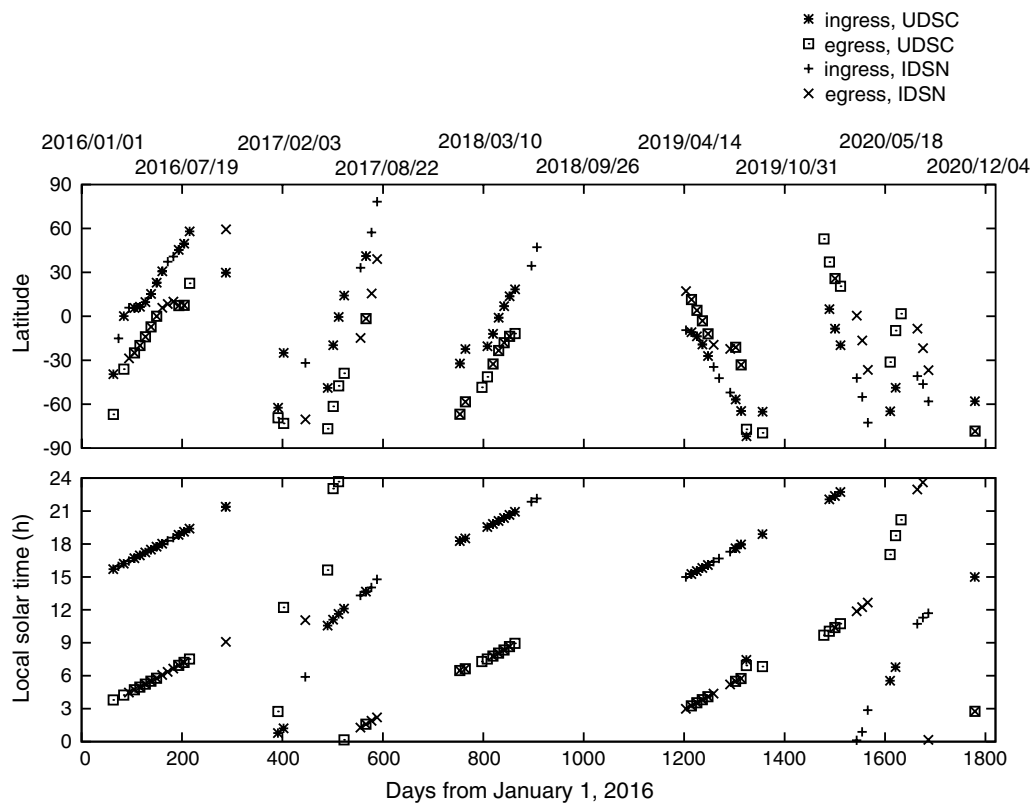


Fig. 2 (Upper) Latitudes and (lower) local solar times of the observation points from January 2016 to December 2020 for the two tracking stations, UDSC of JAXA and ISRN of ISRO

observation point is defined as the tangential point of the straight line between the spacecraft and the ground station at the moment when the spacecraft is occulted by the 70-km-altitude surface of Venus. It should be noted that the observations after July 2017 have not yet been confirmed; time slots for tracking at the ground stations need to be allocated to those opportunities. The first observation was conducted on March 3, 2016, and 10 occultation experiments, including 10 ingress (entry) and 9 egress (exit) measurements, have been conducted by April 2017.

The uniqueness of the Akatsuki RS is that the observation points cluster in the low and middle latitude because of the near-equatorial orbit. Since the onboard cameras are designed to observe wide areas in the low latitude, the locations probed by RS can be observed by the cameras a short time (h) before or after each occultation experiment. Mostly dawn and dusk regions have been probed by April 2017.

Performance of the ultra-stable oscillator

The ultra-stable oscillator (USO) was switched on in June 2010, just after the launch, and has been switched

off from July 2011 to December 2015. To evaluate the stability of the USO output frequency after the launch, downlink signals generated by the USO were recorded several times at UDSC before July 2011 and during the initial checkout phase after December 2015. An analysis of the data showed that the long-term drift of the output frequency was found to be less than $\sim 3 \times 10^{-8}$ times the nominal frequency. The derived Allan deviations are shown in Fig. 3; the frequency stability is $< 10^{-12}$ for the averaging time of 1–1000 s, and no notable degradation is observed after the launch. This stability corresponds to a frequency resolution of ~ 0.01 Hz, which assures discrimination of atmospheric temperature fluctuations with a magnitude of 0.1 K imposed on adjacent two layers separated by 1 km (Imamura et al. 2011).

Signal processing

In the processing of recorded data, we first subtract the Doppler shift calculated from the orbital information and a model atmosphere from the original signal by heterodyning, thereby suppressing the frequency variation and enabling narrow-band filtering. Then, approximate carrier frequencies are determined for successive time

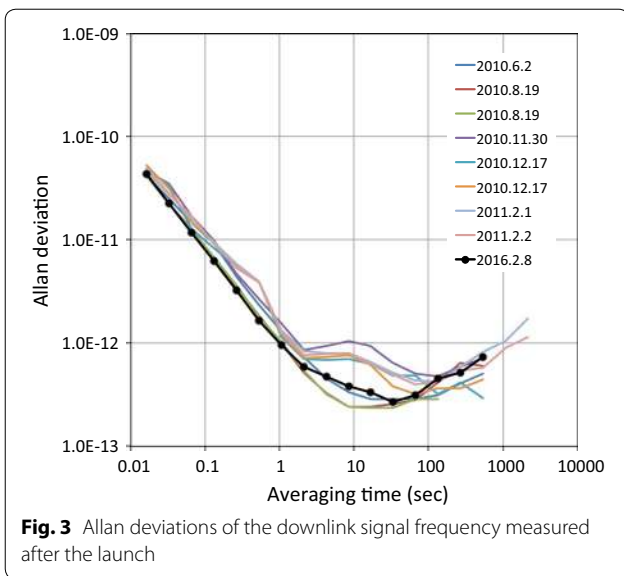


Fig. 3 Allan deviations of the downlink signal frequency measured after the launch

blocks by fitting a theoretical signal spectrum (sinc function) to the discrete Fourier transforms (Lipa and Tyler 1979). The resultant frequency variation is subtracted

from the signal by heterodyning in order to apply another narrow-band filtering. The signal frequency and intensity time series to be used for the analysis of the atmospheric structure are obtained by successively fitting a sinc function to the narrow-band filtered data.

A typical example of the obtained signal intensity time series is shown in the upper panel of Fig. 4. This observation, conducted on May 6, 2016, sampled the region of (longitude, latitude, local time, SZA) = (170°, 10°N, 17:14, 78°) during the ingress and the region of (longitude, latitude, local time, SZA) = (350°, 14°S, 05:14, 102°) during the egress. As the spacecraft is hidden by the Venusian atmosphere as seen from the Earth around 900–1000 s, the signal level drops rapidly due to defocusing and absorption. Noise dominates and no signal is found around 1100–2600 s. As the spacecraft emerges as seen from the Earth around 2700–2800 s, the signal level increases and returns to the original level. The lower panel of Fig. 4 shows the deviation of the measured frequency from the predicted frequency that was calculated using the trajectory information and the VIRA atmospheric profile. This residual frequency originates from the difference between the real atmospheric structure

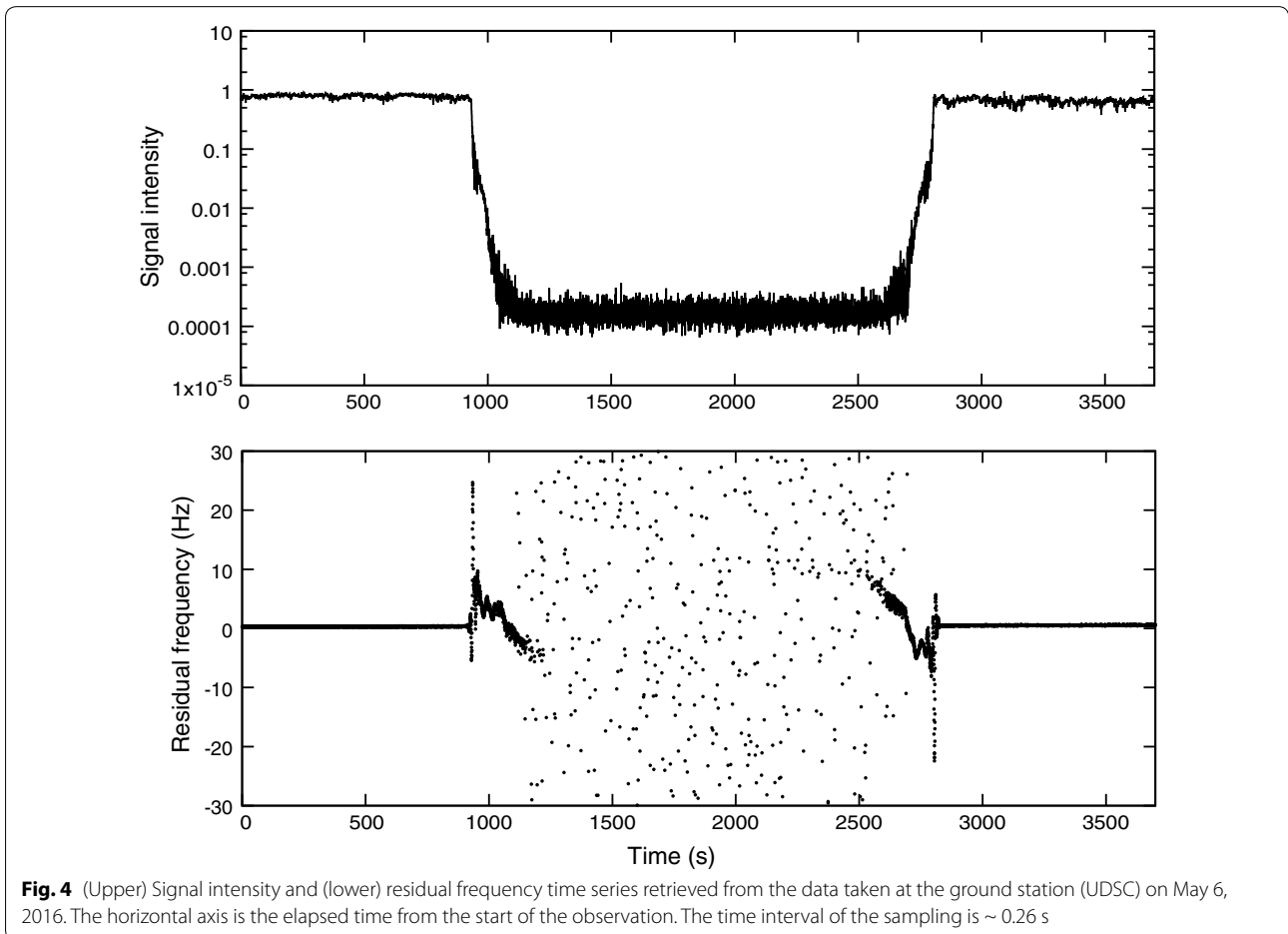


Fig. 4 (Upper) Signal intensity and (lower) residual frequency time series retrieved from the data taken at the ground station (UDSC) on May 6, 2016. The horizontal axis is the elapsed time from the start of the observation. The time interval of the sampling is ~ 0.26 s

and VIRA and is much smaller than the total Doppler shift of > 100 kHz caused by the movements of the spacecraft and the tracking station. The frequency cannot be measured around 1200–2500 s where the signal is too weak.

The sum of the frequency variation in the final product like Fig. 4 and the frequency variation that has been subtracted via heterodyning in the course of the processing gives the total Doppler shift. Subtraction of the “straight-line Doppler shift”, which is the frequency variation to be observed if Venus does not exit, from the total Doppler shift gives the contribution of the Venusian atmosphere termed “atmospheric Doppler shift”. Although the atmospheric Doppler shift should be zero in the portion of the data above the height of the ionosphere, we usually observe a smoothly varying frequency component that is attributed to the error in the trajectory data. To remove this frequency offset, we fit a linear function to this portion of the frequency time series and subtract it from the whole time series; this procedure is termed “baseline fit”. The atmospheric Doppler shift corrected by baseline fit is combined with the trajectory data to calculate the bending angle and the impact parameter.

Figure 5 shows an example of the relationship between the bending angle α and the impact parameter a as well as the relationship between α and the ray closest distance, calculated for the ingress observation conducted on May 6, 2016 (same as Fig. 4). The minimum a corresponds to a height above the surface of ~ 45 km, and the minimum ray closest distance corresponds to a height

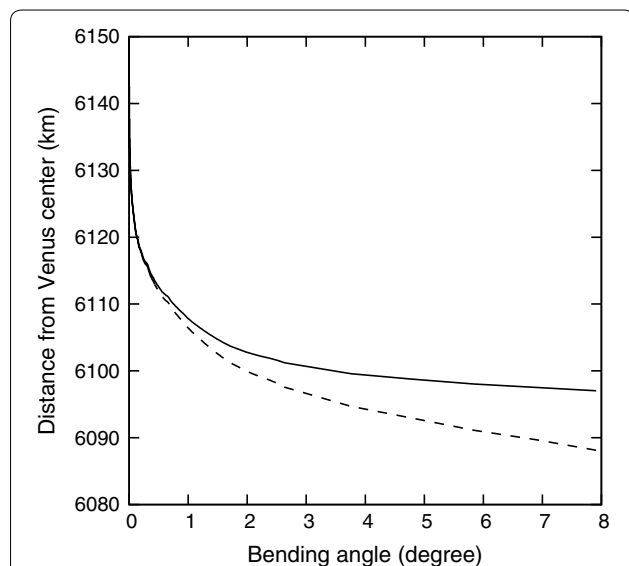


Fig. 5 Relationship between the bending angle and the impact parameter (solid) and that between the bending angle and the ray closest distance (dashed) calculated for the ingress observation conducted on May 6, 2016

of ~ 37 km. The α – a relationship is used to obtain an atmospheric profile through Abel transform (1). For the integration with respect to a in Abel transformation, α needs to be a single-valued function of a . However, α sometimes becomes a multivalued function of a below clouds due to low signal-to-noise ratios. To suppress such multivalued behavior, the integration time is increased in those regions, and extreme outliers are removed by visual inspection.

Atmospheric profiles

The temperature profiles obtained by February 2017 using UDSC are shown in Fig. 6. An observation conducted in March using IDSN is not included because the analysis of the data is ongoing. The upper boundary condition is taken to be $T = 170$ K at $r_{\text{top}} = 6146.8$ km (95 km altitude). The statistical uncertainty in the temperature is estimated to be on the order of 0.1 K for a vertical resolution of 1 km based on the link budget (Imamura et al. 2011); more precise evaluation based on the measured signal-to-noise ratios is ongoing. Two profiles at high latitudes ($> 65^\circ$) were excluded because the closest point along the ray moved over a wide latitudinal range ($> 10^\circ$) during these experiments; such a latitudinal movement of the ray in the high latitude, where the atmospheric structure changes steeply with latitude, might cause large errors in the retrieval that does not consider horizontal variation. The profiles except these are close to VIRA (Seiff et al. 1985), suggesting a remarkable stability of the Venusian atmosphere over decades.

The temperature profiles clearly show differences in the stratification characteristics among the altitude regions.

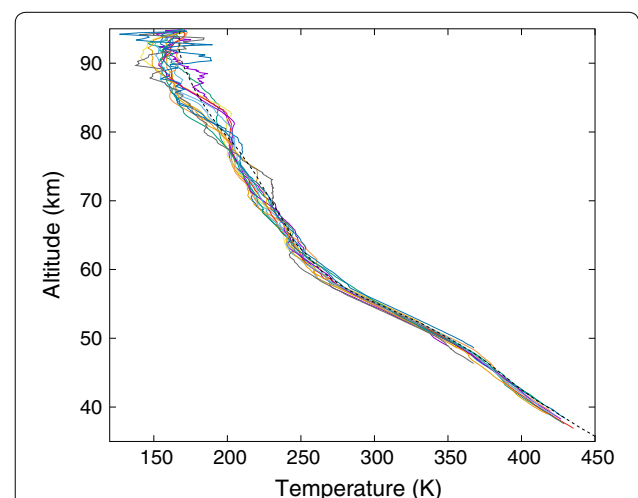


Fig. 6 Temperature profiles obtained by the radio occultation experiments. The VIRA temperature curve profile for the low latitude ($< 30^\circ$) is also plotted by a dashed curve for comparison. The radius of Venus is assumed to be 6051.8 km

Almost constant lapse rate of ~ 10 K/km, which is close to the adiabatic lapse rate (Seiff et al. 1985), is observed in the middle and lower cloud region (50–58 km); this region is considered as a convective layer driven by the heating of the cloud base by the thermal infrared flux from below (Pollack et al. 1980). The region below the cloud (< 50 km) is weakly stable. The region above 58 km is also stable and is dominated by short-vertical scale (< 5 km) fluctuations, being consistent with Venus Express radio occultation experiments (Tellmann et al. 2012). The range of the temperature variation near the top is ~ 50 K, which is smaller than the day-to-day variability of ~ 80 K in the same height region observed by the solar occultation experiment SOIR onboard Venus Express (Mahieux et al. 2012; Limaye et al. 2017). More measurements are needed to better understand the variability.

An advantage of Akatuski RS is a rather dense sampling in the low latitude (Fig. 2). The static stability profiles in the low latitude ($< 40^\circ$) are shown in Fig. 7 for the morning side and the afternoon side separately. The static stability is defined as $dT/dz - \Gamma$, where z is the altitude and Γ is the adiabatic lapse rate calculated from the altitude-dependent specific heat at constant pressure given by Seiff et al. (1985). The altitude-dependent characteristics mentioned above are more evident in this figure. Focusing on the weak stability layer below clouds, the stability reaches a maximum around 45 km altitude and declines with decreasing altitude below this level; this feature was detected by entry probes (Seiff et al. 1980) but has never been observed since then.

Comparing the morning and the afternoon profiles, local time-dependent features are seen at various vertical scales. The amplitudes of the fine structures with vertical scales of < 5 km below 70 km altitude seem to be larger on the morning side, and the phase of the background wavy structure with a vertical scale of > 10 km above 70 km seems to be shifted in altitude between these local time regions. The detail of the local time dependence will be reported elsewhere.

Figure 8 shows an example of the H_2SO_4 vapor profile obtained from the intensity time series in the ingress observation at 10°N conducted on May 6, 2016 (data shown in Fig. 4). The error is smaller than 5 ppm; more accurate evaluation is ongoing. In the derivation, the effect of defocusing loss on the signal intensity that was calculated using the observed atmospheric temperatures, and the effect of antenna mispointing have been corrected. The effect of the absorption by CO_2 on the signal intensity has been subtracted following the method of Oschlisniok et al. (2012). The peak mixing ratio of ~ 10 ppm is consistent with the Mariner 10 radio occultation experiment near the equator (Kolodner

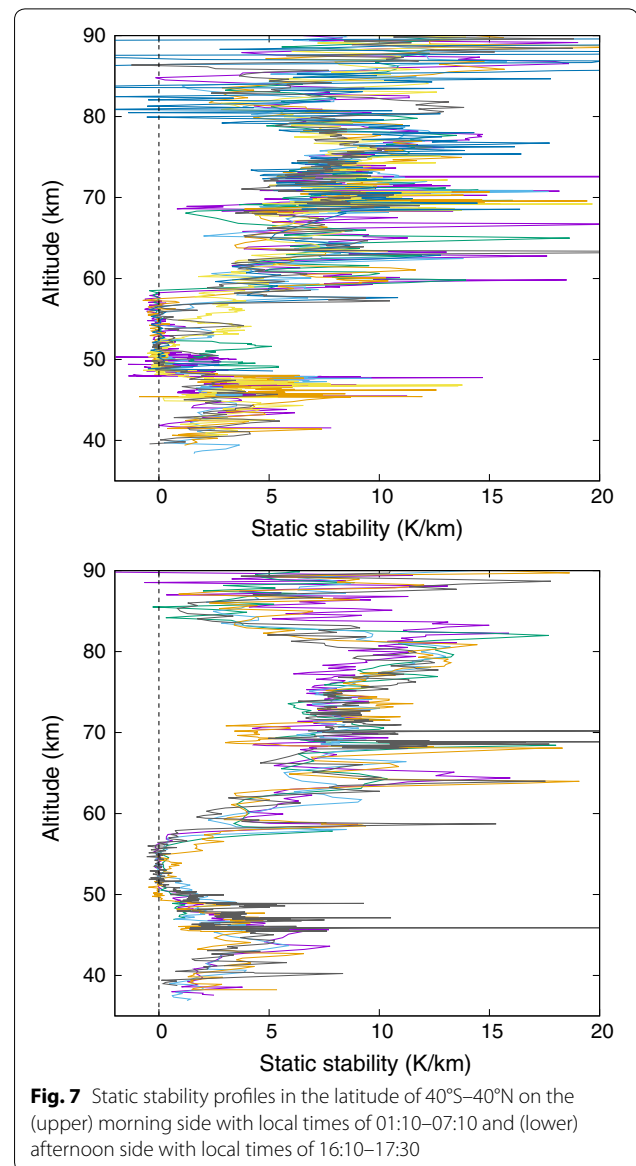


Fig. 7 Static stability profiles in the latitude of 40°S – 40°N on the (upper) morning side with local times of 01:10–07:10 and (lower) afternoon side with local times of 16:10–17:30

and Steffes 1998). At cloud heights (> 47 km), the vapor profile roughly follows the saturation pressure, suggesting equilibrium with the condensed cloud particles. This feature is consistent with Venusian cloud models (James et al. 1997; Imamura and Hashimoto 2001).

Figure 9 shows examples of the ionospheric electron density profiles in an illuminated region and an unilluminated region derived from the ingress and egress observations, respectively, conducted on May 6, 2016 (data shown in Fig. 4). The frequency variation caused by the ionosphere is much smaller than that by the neutral atmosphere, and the electron density profile is generally sensitive to short-timescale noise that cannot be removed by baseline fit. However, at least in this

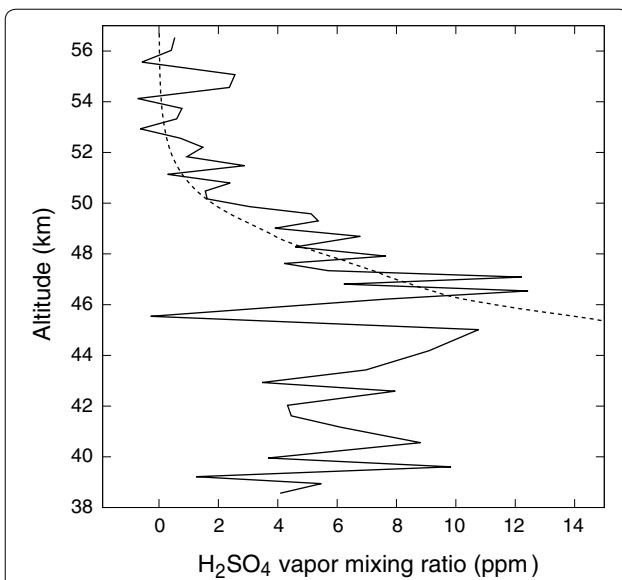


Fig. 8 An example of the H_2SO_4 vapor mixing ratio profile obtained from the ingress occultation at 10°N conducted on May 6, 2016 (solid). The mixing ratios corresponding to the saturation vapor pressure for the observed temperature are also plotted for comparison (dotted)

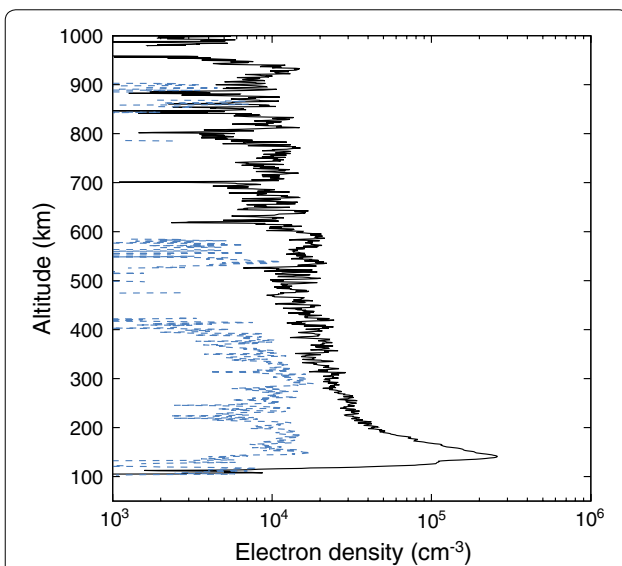


Fig. 9 Electron density profile obtained from the ingress occultation (solid) that sampled an illuminate region ($\text{SZA} = 78^\circ$) and the profile from the egress occultation (blue dashed) that sampled an unilluminated region ($\text{SZA} = 102^\circ$) conducted on May 6, 2016

example, the baseline fit is successful and the remaining small-scale variations seem to be smaller than the peak frequency variation cause by the ionosphere. The peak electron density of $\sim 3 \times 10^5 \text{ cm}^{-3}$ and the peak altitude of $\sim 140 \text{ km}$ in the illuminated region are typical of the

dayside ionosphere. Above 200 km altitude in the illuminated region, the electron density gradually decreases with height and merges into the background noise floor, which is around 10^4 cm^{-3} . The electron density in the unilluminated region is marginally detectable at 100–400 km altitudes. The overall features are consistent with the previous observations (Kliore and Luhmann 1991; Pätzold et al. 2007).

Summary

Radio occultation observation of the Venusian atmosphere in the Akatsuki mission has started in March 2016. Ten occultation experiments, including 10 ingress and 9 egress measurements, have been conducted by February 2017. From the open-loop recorded data, the altitude distributions of the temperature, the H_2SO_4 vapor mixing ratio, and the electron density are being successfully retrieved.

The dataset will be used for a variety of scientific researches. The temperature and H_2SO_4 vapor profiles are analyzed in combination with cloud images obtained successively from Akatsuki and also with cloud-tracked vectors obtained from those images. Complementary uses of those data enables studies on the interaction between cloud physics and thermal structure, the three-dimensional structures of atmospheric circulation and waves, and the vertical coupling between the cloud-level atmosphere and the mesosphere. The combination of the electron density profiles with the whole Akatsuki dataset will provide clues to the role of the variation of the neutral atmosphere in the variability of the ionosphere. Comparison of Akatsuki RS results with the previous radio occultation results from Pioneer Venus (Kliore and Patel 1980) and Venus Express (Pätzold et al. 2007; Tellmann et al. 2009) would reveal long-term variation of the Venusian atmosphere. The radio occultation temperatures are used in the radiative transfer calculation for the analyses of data taken by ground-based telescopes. The results from those studies will be presented in separate papers.

Apart from Venus researches, radio occultation observations of the solar corona were conducted during the solar conjunction periods in June–July 2011 and May–June 2016. The outward flow velocity can be retrieved from the signal intensity fluctuation, and the plasma density fluctuation can be retrieved from the frequency fluctuation. The 2011 observation has revealed the radial profile of the flow velocity (Imamura et al. 2014b), the radial distribution of compressible waves (Miyamoto et al. 2014), and the internal structure of a coronal mass ejection (Ando et al. 2015a, b).

Authors' contributions

TI is the principal investigator of the experiment. HA, ST and JO contributed to data analysis. MP, BH, YM, HT, TT, AT, ZY, IN, TH and MN contributed to the

development of the observation system. KN, YF, SL, TA, HN and TI contributed to science planning. AY, TS, TS, CH, TF, KO, KS, HK, SO, ST, MY, MS and LY contributed to command planning and spacecraft operation. TI represents the orbital dynamics team. SM, YY, NH and GLH contributed to data archiving. RKC represents the ISRO RS Team. All authors read and approved the final manuscript.

Author details

¹ Graduate School of Frontier Sciences, The University of Tokyo, Kiban-tou 4H7, 5-1-5 Kashiwanoha, Kashiwa, Chiba 277-8561, Japan. ² Faculty of Science, Kyoto Sangyo University, Motoyama, Kamigamo, Kita-ku, Kyoto 603-8555, Japan. ³ Abteilung Planetenforschung, Rheinisches Institut für Umweltforschung, Universität zu Köln, Cologne, Germany. ⁴ Institut für Raumfahrttechnik und Weltraumnutzung, Universität der Bundeswehr München, Neubiberg, Germany. ⁵ Institute of Space and Astronautical Science, Japan Aerospace Exploration Agency, 3-1-1, Yoshinodai, Chuo-ku, Sagami-hara 252-5210, Japan. ⁶ Faculty of Science, Nara Women's University, Kita-uoya Nishi-machi, Nara 630-8506, Japan. ⁷ Swedish Institute of Space Physics, Box 812, 981 28 Kiruna, Sweden. ⁸ Space Science and Engineering Center, University of Wisconsin, Madison, WI, USA. ⁹ Space Physics Laboratory, Vikram Sarabhai Space Center, Thumba PO, Trivandrum 695 022, India. ¹⁰ National Astronomical Observatory of Japan, 2-21-1 Osawa, Mitaka, Tokyo 181-8588, Japan. ¹¹ College of Science, Rikkyo University, 3-34-1 Nishi-Ikebukuro, Toshima-ku, Tokyo 171-8501, Japan. ¹² The University of Shiga Prefecture, 2500, Hassaka-cho, Hikone-City, Shiga 522-8533, Japan. ¹³ National Institute of Technology, Matsue College, 14-4 Nishiikuma-cho, Matsue, Shimane 690-8518, Japan. ¹⁴ Center for Planetary Science/Department of Planetology, Kobe University, 7-1-48, Minatogima-Minamimachi, Chuo-ku, Kobe 650-0047, Japan. ¹⁵ Senshu University, 2-1-1 Higashimita, Tama-ku, Kawasaki, Kanagawa 214-8580, Japan. ¹⁶ Tokai University, Research and Information Center, 4-1-1 Kitakaname, Hiratsuka-shi, Kanagawa 259-1292, Japan. ¹⁷ The University of Aizu, Aizu-Wakamatsu, Fukushima 965-8580, Japan. ¹⁸ Department of Earth Sciences, Okayama University, 3-1-1 Tsushimanaka, Kita-ku, Okayama 700-8530, Japan. ¹⁹ Planetary Exploration Research Center, Chiba Institute of Technology, 2-17-1 Tsudanuma, Narashino, Chiba 275-0016, Japan. ²⁰ Japan Aerospace Exploration Agency, 2-1-1 Sengen, Tsukuba, Ibaraki 305-8505, Japan.

Acknowledgements

We would like to acknowledge all members of the Akatsuki project team and the staff of UDSC for supporting the preparation of the experiment. The high performance of the USO was achieved by the tremendous efforts made by Theo Schwall, Wolfgang Schäfer and other engineers of TimeTech GmbH. We thank Richard Simpson at Stanford University and Kevin McGouldrick at University of Colorado, Boulder for supporting data archiving. We also thank Koh-ichiro Oyama for continuous encouragement.

Competing interests

The authors declare that they have no competing interests.

Availability of data and materials

The radio occultation data used in this study will become open to the public at DARTS (Data ARchives and Transmission System) of JAXA and the PDS (Planetary Data System) of NASA.

Consent for publication

Not applicable

Ethics approval and consent to participate

Not applicable.

Funding

This work was supported by JSPS KAKENHI Grant Nos. JP22244060, JP24540482, JP16H04060, JP00706335 and JP16H02231.

Publisher's Note

Springer Nature remains neutral with regard to jurisdictional claims in published maps and institutional affiliations.

Received: 4 July 2017 Accepted: 20 September 2017

Published online: 03 October 2017

References

- Ando H, Imamura T, Tsuda T, Tellmann S, Pätzold M, Häusler B (2015a) Vertical wavenumber spectra of gravity waves in the Venus atmosphere obtained from Venus Express radio occultation data: evidence for saturation. *J Atmos Sci* 72:2318–2329. doi:10.1175/JAS-D-14-0315.1
- Ando H, Shiota D, Imamura T, Tokumaru M, Asai A, Isobe H, Pätzold M, Häusler B, Nakamura M (2015b) Internal structure of a coronal mass ejection revealed by Akatsuki radio occultation observations. *J Geophys Res* 120:5318–5328. doi:10.1002/2015JA021076
- Eshleman VR (1973) The radio occultation method for the study of planetary atmospheres. *Planet Space Sci* 21:1521–1531
- Essen L, Froome KD (1951) The refractive indices and dielectric constants of air and its principal constituents at 24,000 Mc/s. *Proc Phys Soc London Sect B* 64:862–875. doi:10.1088/0370-1301/64/10/303
- Fjeldbo G, Eshleman VR (1968) The atmosphere of Mars analyzed by integral inversion of the Mariner IV occultation data. *Planet Space Sci* 16:1035–1059
- Fjeldbo G, Kliore AJ, Eshleman VR (1971) The neutral atmosphere of Venus as studied with the Mariner V radio occultation experiments. *Astron J* 76:123–140
- Häusler B, Pätzold M, Tyler GL, Simpson RA, Bird MK, Dehant V, Barriot J-P, Eidel W, Mattei R, Remus S, Selle J, Tellmann S, Imamura T (2006) Radio science investigations by VeRa onboard the Venus Express spacecraft. *Planet Space Sci* 54:1315–1335
- Häusler B, Pätzold M, Tyler G L, Simpson R A, Hinson D, Bird M K, Treumann R A, Dehant V, Eidel W, Remus S, Selle J (2007) Atmospheric, ionospheric, surface, and radio wave propagation studies with the Venus Express radio science experiment VeRa. ESA Scientific Publication, ESA-SP-1295, pp 1–30
- Hinson DP, Jenkins JM (1995) Magellan radio occultation measurements of atmospheric waves on Venus. *Icarus* 114:310–327
- Imamura T, Hashimoto GL (1998) Venus cloud formation in the meridional circulation. *J Geophys Res* 103:31349–31366
- Imamura T, Hashimoto GL (2001) Microphysics of Venusian clouds in rising tropical air. *J Atmos Sci* 58:3597–3612
- Imamura T, Iwata T, Yamamoto Z, Mochizuki N, Kono Y, Matsumoto K, Liu Q, Noda H, Hanada H, Oyama K-I, Nabatov A, Futaana Y, Saito A, Ando H (2010) Studying the lunar ionosphere with SELENE radio science experiment. *Space Sci Rev* 154:305–316
- Imamura T, Toda T, Tomiki A, Hirahara D, Hayashiyama T, Mochizuki N, Yamamoto Z, Abe T, Iwata T, Noda H, Futaana Y, Ando H, Häusler B, Pätzold M, Nabatov A (2011) RS: Radio Science investigation of the Venus atmosphere and ionosphere with Venus orbiter, Akatsuki. *Earth Planets Space* 63:493–501. doi:10.5047/eps.2011.03.009
- Imamura T, Nabatov A, Mochizuki N, Iwata T, Hanada H, Matsumoto K, Noda H, Kono Y, Liu Q, Futaana Y, Ando H, Yamamoto Z, Oyama K-I, Saito A (2012) Radio occultation measurement of the electron density near the lunar surface using a subsatellite on the SELENE mission. *J Geophys Res* 117:A06303. doi:10.1029/2011JA017293
- Imamura T, Higuchi T, Maejima Y, Takagi M, Sugimoto N, Ikeda K, Ando H (2014a) Inverse insolation dependence of Venus' cloud-level convection. *Icarus* 228:181–188
- Imamura T, Tokumaru M, Isobe H, Shiota D, Ando H, Miyamoto M, Toda T, Häusler B, Pätzold M, Nabatov A, Asai A, Yaji K, Yamada M, Nakamura M (2014b) Outflow structure of the quiet Sun corona probed by spacecraft radio scintillations in strong scattering. *Astrophys J* 788:117(10pp). doi:10.1088/0004-637X/788/2/117
- James EP, Toon OB, Schubert G (1997) A numerical microphysical model of the condensational Venus cloud. *Icarus* 129:147–171
- Jenkins JM, Steffes PG, Hinson DP, Twicken JD, Tyler GL (1994) Radio occultation studies of the Venus atmosphere with the Magellan spacecraft. 2. Results from the October 1991 experiments. *Icarus* 110:79–93
- Kliore AJ, Luhmann JG (1991) Solar cycle effects on the structure of the electron density profiles in the dayside ionosphere of Venus. *J Geophys Res* 96:21281–21289
- Kliore AJ, Patel IR (1980) Vertical structure of the atmosphere of Venus from Pioneer Venus orbiter radio occultations. *J Geophys Res* 85:7957–7962
- Kolodner MA, Steffes PG (1998) The microwave absorption and abundance of sulfuric acid vapor in the Venus atmosphere based on new laboratory measurements. *Icarus* 132:151–169

- Krasnopolsky VA, Pollack JB (1994) H_2O – H_2SO_4 system in Venus' clouds and OCS, CO, and H_2SO_4 profiles in Venus' troposphere. *Icarus* 109:58–78
- Leroy SS, Ingersoll AP (1996) Radio scintillations in Venus's atmosphere: application of a theory of gravity wave generation. *J Atmos Sci* 53:1018–1028
- Limaye SS et al (2017) The thermal structure of the Venus atmosphere: inter-comparison of Venus Express and ground based observations of vertical temperature and density profiles. *Icarus* 294:124–155. doi:[10.1016/j.icarus.2017.04.020](https://doi.org/10.1016/j.icarus.2017.04.020)
- Lipa B, Tyler L (1979) Statistical and computational uncertainties in atmospheric profiles from radio occultation: Mariner 10 at Venus. *Icarus* 39:192–208
- Mahieux A, Vandaele AC, Robert S, Wilquet V, Drummond R, Montmessin F, Bertaux JL (2012) Densities and temperatures in the Venus mesosphere and lower thermosphere retrieved from SOIR on board Venus Express: carbon dioxide measurements at the Venus terminator. *J Geophys Res* 117:E07001. doi:[10.1029/2012JE004058](https://doi.org/10.1029/2012JE004058)
- McGouldrick K, Toon OB (2008a) Modeling the effects of shear on the evolution of the holes in the condensational clouds of Venus. *Icarus* 196:35–48
- McGouldrick K, Toon OB (2008b) Observable effects of convection and gravity waves on the Venus condensational cloud. *Planet Space Sci* 46:1112–1131
- McGouldrick K, Momary TW, Baines KH, Grinspoon DH (2012) Quantification of middle and lower cloud variability and mesoscale dynamics from Venus Express/VIRTIS observations at 1.74 μm . *Icarus* 217:615–628. doi:[10.1016/j.icarus.2011.07.009](https://doi.org/10.1016/j.icarus.2011.07.009)
- Miyamoto M, Imamura T, Tokumaru M, Ando H, Isobe H, Asai A, Shiota D, Toda T, Häusler B, Pätzold M, Nabatov A, Nakamura M (2014) Radial distribution of compressive waves in the solar corona revealed by Akatsuki radio occultation observations. *Astrophys J* 797(1):51. doi:[10.1088/0004-637X/797/1/51](https://doi.org/10.1088/0004-637X/797/1/51)
- Nakamura M, Imamura T, Ishii N, Abe T, Satoh T, Suzuki M, Ueno M, Yamazaki A, Iwagami N, Watanabe S, Taguchi M, Fukuhara T, Takahashi Y, Yamada M, Hoshino N, Ohtsuki S, Uemizu K, Hashimoto GL, Takagi M, Matsuda Y, Ogohara K, Sato N, Kasaba Y, Kouyama T, Hirata N, Nakamura R, Yamamoto Y, Okada N, Horinouchi T, Yamamoto M, Hayashi Y (2011) Overview of Venus orbiter, Akatsuki. *Earth Planets Space* 63:443–457. doi:[10.5047/eps.2011.02.009](https://doi.org/10.5047/eps.2011.02.009)
- Nakamura M et al (2016) AKATSUKI returns to Venus. *Earth Planets Space* 68:75. doi:[10.1186/s40623-016-0457-6](https://doi.org/10.1186/s40623-016-0457-6)
- Newman M, Schubert G, Kliore AJ, Patel IR (1984) Zonal winds in the middle atmosphere of Venus from Pioneer Venus radio occultation data. *J Atmos Sci* 41:1901–1913
- Oschlisniok J, Häusler B, Pätzold M, Tyler GL, Bird MK, Tellmann S, Remus S, Andert T (2012) Microwave absorptivity by sulfuric acid in the Venus atmosphere: first results from the Venus Express Radio Science experiment VeRa. *Icarus* 221:940–948
- Pätzold M, Häusler B, Bird MK, Tellmann S, Mattei R, Asmar SW, Dehant V, Eidel W, Imamura T, Simpson RA, Tyler GL (2007) The structure of Venus' middle atmosphere and ionosphere. *Nature* 450:657–660
- Piccialli A, Tellmann S, Titov DV, Limaye SS, Khatuntsev IV, Pätzold M, Häusler B (2012) Dynamical properties of the Venus mesosphere from the radio-occultation experiment VeRa onboard Venus Express. *Icarus* 217:669–681
- Pollack JB, Toon OB, Boese R (1980) Greenhouse models of Venus' high surface temperature, as constrained by Pioneer Venus measurements. *J Geophys Res* 85:8223–8231
- Seiff A, Kirk DB, Young RE, Blanchard RC, Findlay JT, Kelly GM, Sommer SC (1980) Measurements of thermal structure and thermal contrasts in the atmosphere of Venus and related dynamical observations: Results From the four Pioneer Venus Probes. *J Geophys Res* 85:7903–7933
- Seiff A, Schofield JT, Kliore AJ, Taylor FW, Limaye SS et al (1985) Models of the structure of the middle atmosphere of Venus from the surface to 100 kilometers altitude. *Adv Space Res* 5(11):1–305
- Tellmann S, Pätzold M, Häusler B, Bird MK, Tyler GL (2009) Structure of the Venus neutral atmosphere as observed by the Radio Science experiment VeRa on Venus Express. *J Geophys Res* 114:E00B36. doi:[10.1029/2008JE003204](https://doi.org/10.1029/2008JE003204)
- Tellmann S, Häusler B, Hinson DP, Tyler GL, Andert TP, Bird MK, Imamura T, Pätzold M, Remus S (2012) Small-scale temperature fluctuations seen by the VeRa radio science experiment on Venus Express. *Icarus* 221:471–480
- Toda T, Hayashiyama T, Kamata Y, Ishii N, Nakamura M (2010) Flight model development of PLANET-C telecommunication subsystem. In: The 27th international symposium on space technology and science, transactions of japan society for aeronautical and space sciences, space technology Japan 8, No. ists27:Tj_17-Tj_22
- Tyler GL (1987) Radio propagation experiments in the outer solar system with Voyager. *Proc IEEE* 75:1404–1431
- Woo R, Armstrong JW, Ishimaru A (1980) Radio occultation measurements of turbulence in the Venus atmosphere by Pioneer Venus. *J Geophys Res* 85:8031–8038

Submit your manuscript to a SpringerOpen® journal and benefit from:

- Convenient online submission
- Rigorous peer review
- Open access: articles freely available online
- High visibility within the field
- Retaining the copyright to your article

Submit your next manuscript at ► springeropen.com
